Role of Zinc in the Structure and Toxic Activity of Botulinum Neurotoxin†

Fen-Ni Fu,‡ Richard B. Lomneth,§ Shuowei Cai,‡ and Bal Ram Singh*,‡,||

Department of Chemistry and Biochemistry, University of Massachusetts Dartmouth, Dartmouth, Massachusetts 02747, and Department of Chemistry, University of Nebraska at Omaha, Omaha, Nebraska 68182

Received September 26, 1997; Revised Manuscript Received January 27, 1998

ABSTRACT: Zn^{2+}-protease activity of botulinum neurotoxin causes the blockage of neurotransmitter release resulting in botulism disease. We have investigated the role of Zn^{2+} in the biological activity of type A botulinum neurotoxin by removing the bound Zn^{2+} by EDTA treatment, followed by monitoring its structure in terms of secondary and tertiary folding (second derivative UV, FT-IR, and circular dichroism spectroscopy) and function in terms of its effect on the release of norepinephrine from PC12 cells. The single Zn^{2+} bound to each neurotoxin molecule was reversibly removed by EDTA treatment, whereas the biological activity of the neurotoxin was irreversibly lost. Based on the Amide III IR spectral analysis, the α-helical content of neurotoxin increased from 29% to 42% upon removal of Zn^{2+}, which reverted to 31% upon treatment with 1:5 molar excess of exogenous Zn^{2+}. Second derivative UV spectroscopy revealed no change in surface topography of Tyr residues with removal of Zn^{2+}. However, near-UV circular dichroism signals suggested significant alterations in the topography of Phe and Tyr residues that could be buried in the protein matrix. Thermal unfolding experiments suggested that removal of Zn^{2+} results in the formation of the molten globule-like structure of type A botulinum neurotoxin. Tertiary structural changes introduced by Zn^{2+} removal were irreversible, which correlated well with the irreversibility of the biological activity of the neurotoxin. On the basis of these results, we suggest that Zn^{2+} plays a significant structural role in addition to its catalytic role in Zn^{2+}-protease activity of type A botulinum neurotoxin.

Botulinum neurotoxins (BoNTs) are a family of seven structurally similar but antigenically different proteins produced by different strains of *Clostridium botulinum*. These proteins are the most toxic substance known (LD_{50} < 0.3 ng/kg) and specifically act on the neuromuscular junctions to block acetylcholine release. Such a blockage leads to flaccid paralysis in botulism disease (*1*). BoNTs are also being used as therapeutic agents to treat several neuromuscular disorders such as strabismus, blepherospasm, and torticollis (*2*). In recent years, BoNTs have received unusual attention because of their ability to block exocytosis not only in neuronal tissues but also in other tissues, which allows their use as tools to investigate the mechanism of the exocytosis process in general (*3*).

BoNTs are produced as 150 kDa single-chain polypeptides which can be nicked by endogenous or exogenous proteases into two subunit chains (a 100 kDa heavy chain and a 50 kDa light chain) linked through a disulfide bond (*4*). The heavy (H) chain is mainly involved in the cell binding, internalization, and translocation of the BoNT into nerve cells where the light (L) chain exhibits its intracellular toxic activity (*4*−*6*). BoNTs possess a unique zinc-binding motif (HExxH) in the central region of the L chain subunit polypeptide, which is typical of a zinc metalloprotease (*7, 8*). The essential Zn^{2+} is suggested to be coordinated by two histidines and a water bound to the glutamate in the motif (*9, 10*). The fourth ligand, presumably a glutamate, has not yet been identified and could be distally located.

Zinc present in proteins can play a structural or a catalytic role (*8*). Based on a comparison with thermolysin, a zinc protease in which Zn^{2+} is coordinated by two histidines, a bound water at the glutamate residue of HExxH motif and a fourth glutamate ligand located 25 residues toward C-terminal end; the Zn^{2+} in BoNT is suggested to be catalytic in nature (*11*). However, in view of the absence of the fourth ligand in a similar position as in thermolysin, the presence of Zn^{2+} could maintain structures in BoNT that are likely to be critical for its functional activity. Such a feature is particularly important for BoNT, as each of the BoNT serotypes has unique substrate and cleavage site (*4, 5*) despite identical zinc-binding motifs in all of the serotypes. Zn^{2+}-binding could be involved in defining differential specificity of BoNT serotypes to different substrates and cleavage sites.

In this study, we have investigated the role of bound Zn^{2+} on the structure of BoNT/A and its relation to neurotoxin function in terms of blockage of neurotransmitter release in PC12 cells. Removal of Zn^{2+} inactivates the neurotoxin irreversibly. Structural changes at the secondary and tertiary levels accompanying the Zn^{2+} removal were also essentially irreversible. Analysis of Zn^{2+} in native and Zn^{2+}-replenished apo-neurotoxin suggested that there was one Zn^{2+} ion bound

† This study was in part supported by a NIH-National Institute of Neurological Disorders and Stroke Grant NS33740.

* Author to whom correspondence should be addressed at Department of Chemistry and Biochemistry, University of Massachusetts Dartmouth, 285 Old Westport Road, Dartmouth, MA 02747. Phone: 508-999-8588. Fax: 508-999-8451. E-mail: bsingh@umassd.edu.

‡ University of Massachusetts Dartmouth.

§ University of Nebraska at Omaha.

|| The Henry Dreyfus Teacher−Scholar.

S0006-2960(97)02396-9 CCC: $15.00 © 1998 American Chemical Society
Published on Web 03/26/1998

to each BoNT/A molecule, and the binding of Zn^{2+} itself was a reversible process.

MATERIALS AND METHODS

Neurotoxin Preparation. C. botulinum (strain Hall) stock culture was grown in N-Z amine-based growth medium according to the procedures described by Fu et al. (*12*) with only minor modifications. Briefly, the culture after 4-day growth was acid precipitated, digested with RNAase, and precipitated again with ammonium sulfate (0.35 g/mL). The precipitate was resuspended to obtain crude extract. The neurotoxin was purified from the crude extract using a series of chromatographic columns including a DEAE-A-50 Sephadex column (equilibrated at pH 5.5), Sephadex G-100 column (equilibrated at pH 5.5), and another DEAE-A-50 Sephadex column (equilibrated at pH 7.9). The neurotoxin recovered was slightly impure and was further purified on a SP Sephadex C-50 column (equilibrated at pH 7.0) using 0−0.5 M NaCl gradient elution. The purity of BoNT/A thus obtained was checked with the sodium dodecyl sulfate−polyacrylamide gel electrophoresis (SDS−PAGE). Pure BoNT/A preparations showed a single band at approximately 145 kDa with Coomassie Blue staining on SDS−PAGE gel run under nonreducing conditions. Under reducing conditions, two bands representing the light and heavy chains of pure BoNT/A were observed on the SDS−PAGE gel. Purified BoNT/A was stored at 4 °C after precipitation with ammonium sulfate.

Preparation of Apo- and Zn^{2+}-Replenished BoNT/A. Zn^{2+} removal from BoNT samples was carried out according to the procedure described by Schiavo et al. (*9*). All the buffers were prepared with HPLC-grade water to eliminate the presence of any trace heavy metals (conductance 1.9 μmho/cm). The ammonium sulfate precipitate of BoNT/A was dissolved in 150 mM Tris-HCl buffer, pH 7.4, to obtain a final concentration of about 1 mg/mL (determined by absorbance at 278 nm with an extinction coefficient of 1.63 cm^2/mg). The sample was extensively dialyzed against the same buffer to remove the ammonium sulfate. A portion of the sample was set aside to be used as a positive control, namely the holo-BoNT/A. The remainder of the dialyzed BoNT sample was then incubated with ethylenediaminetetraacetate (EDTA) at a final concentration of 10 mM for 1 h at 37 °C. EDTA-treated sample (apo-neurotoxin) was extensively dialyzed against 150 mM Tris-HCl buffer, pH 7.4, to remove all excess EDTA as well as Zn^{2+}−EDTA complex. The Zn^{2+}-replenished BoNT/A was obtained by incubating the apo-neurotoxin with a desired concentration of $ZnCl_2$ for an hour at 37 °C, followed by extensive dialysis to remove unbound Zn^{2+}.

Determination of Zinc Content; Atomic Absorption Spectroscopy. All the materials (glassware, dialysis bag, etc.) used in zinc determination experiments were rinsed with HPLC-grade water prior to use. All chemicals used were ultrapure grade and HPLC-grade water was used for all solutions. Before zinc determination, the BoNT/A was extensively dialyzed at 4 °C against 150 mM Tris-HCl buffer, pH 7.4. The protein concentration was determined by absorbance at 278 nm with an extinction coefficient of 1.63 cm^2/mg. The protein sample and dialyzed buffer were analyzed for zinc content using a Perkin-Elmer 5100 PC atomic absorption spectrophotometer with HGA-600 graphic furnace and AS-60 autosampler. The wavelength was set at 213.9 nm, the atomization temperature was set at 1800 °C with the atomization time 3 s. Background correction was performed by using Perkin-Elmer 5100 Zeeman background corrector. The standard series of zinc were prepared by using the zinc reference solution (1000 ppm ±1%) from Fisher Scientific (Fair Lawn, NJ). The linear range of the standard curve was obtained for 0−4 ppb zinc concentration. The protein sample was diluted using the 150 mM Tris-HCl buffer, pH 7.4, so that the zinc content in the protein solution was in the linear range of standard curve. The sample volume of 20 μL was injected through the AS-60 autosampler. The dialyzed buffer was analyzed and used as a blank for protein sample. The zinc content of apo-BoNT/A and zinc-replenished BoNT/A was determined in an identical manner as described above for BoNT/A, using their respective dialyzed buffer solutions as blanks.

Biological Activity Assay. The intracellular action of BoNT/A was investigated by measuring the ^{3}H-labeled-norepinephrine ([^{3}H]NE) release in mechanically permeabilized PC12 cells as described earlier (*13*). Briefly, PC12 cells incubated overnight in a medium containing [^{3}H]NE were permeabilized using a ball homogenizer, incubated on ice for 1 h to allow soluble cytosolic components to diffuse out of the cell, and washed by centrifugation. The permeabilized PC12 cells maintained all structural components to remain competent for exocytosis. Permeabilized cells were incubated for 5 min at 30 °C in the presence of 2 mM MgATP, rat brain cytosol (containing soluble factors necessary for exocytosis), and BoNT/A (or control buffer) to allow BoNT/A to act. Then 1 μM free Ca^{2+} was added to trigger exocytosis, and cells were incubated an additional 15 min at 30 °C. Cell suspensions were pelleted by centrifugation, supernatants were removed, and [^{3}H]NE was measured by scintillation counting. Select cell pellets were also harvested to determine the amount of [^{3}H]NE remaining in cells to determine the percent [^{3}H]NE release.

Secondary Structure Analysis. The effect of Zn^{2+} on the secondary structure of BoNT/A was analyzed by both FT-IR and circular dichroism (CD) spectroscopy.

FT-IR Spectroscopy. The IR spectra were recorded using a Nicolet 8210 FT-IR spectrometer (Nicolet Corp., Madison, WI) using a procedure described in detail previously (*14*). All samples (holo-, apo-, and Zn^{2+}-replenished BoNT/A at a concentration of 1 mg/mL) were applied to the sample compartment made of a 60° horizontal zinc selenide ATR (attenuated total reflectance) crystal. Spectra were collected with 256 coadded scans at 2 cm^{-1} resolution, and a 9 point Savitsky-Golay smoothing was applied. Protein spectra were generated after subtraction of appropriate reference spectra. The subtraction factor was judged by obtaining a flat baseline at 2000−1720 cm^{-1} and a leveled signal at 800−600 cm^{-1}. Both amide I and amide III spectral regions of BoNT spectra were analyzed using the LC program from LabCalc (Galactic Industries Co., Salem, NH) with minor modifications of the method described by Fu et al. (*14*). Deconvolution spectra were obtained with a γ factor of about 2.5 and a filter factor of about 0.35, and were curve-fitted. The parameters obtained from curve-fitting of the deconvolution were used to fit the original BoNT spectra. The resultant underlying peaks were then used to define the secondary structure of BoNT according to the assignments used by Fu et al. (*14*).

Circular Dichroism. CD spectra were recorded on a Jasco J715 spectropolarimeter equipped with a Peltier-type temperature control system (Model PTC-348W). All samples for far-UV CD spectral recording were directly prepared in HPLC-grade water in order to record the spectra down to the vacuum UV region where the presence of salt interfered with the protein spectrum. BoNT/A solutions were extensively dialyzed against the HPLC-grade water. Far-UV CD spectra between 260 and 170 nm were recorded at room temperature in a 1 mm path-length quartz cell using a protein concentration of about 0.2 mg/mL. The scan rate was 20 nm/min with the response time set at 8 s. Equilibrated dialysis water samples after the last change corresponding to different BoNT/A samples were used to record reference spectra under conditions identical to those used for the sample spectral recordings. Reference spectra were subtracted from respective BoNT/A spectra (holo-, apo-, and Zn^{2+}-replenished) to obtain final protein spectra. Secondary structure estimation from far-UV CD spectral data was carried out using a computer program based on the method of Sreerama and Woody (*15*).

Tertiary Structural Analysis. Tertiary structural parameters of BoNT/A in the presence and absence of bound Zn^{2+} were examined in terms of the topography of Trp, Tyr, and Phe (near-UV CD and second derivative UV absorption spectroscopy) and in terms of temperature-induced unfolding (far-UV CD).

Near-UV CD. Near-UV CD spectra (340−240 nm) were recorded with 1.5 mg/mL BoNT concentration in a 1 cm path-length quartz cell at room temperature (25 °C). Scan speed and response time were the same as those used for the far-UV CD recordings described above.

Second Derivative UV Spectroscopy. Absorption spectra of holo-, apo-, and Zn^{2+}-replenished BoNT/A were recorded between 240 and 320 nm using an Uvikon UV/vis spectrophotometer (Model 9410, Kontron Instruments) at room temperature (25 °C). To obtain a spectrum, 5 independent scans were recorded with a 3 nm spectral band at a resolution of 0.5 nm and were averaged. The averaged spectra were derivatized to the second order. The degree of Tyr exposure, α, was estimated according to the method of Ragone et al. (*16*) as described previously (*17*):

$$\alpha = (\gamma_n - \gamma_a)/(\gamma_u - \gamma_a)$$

where, γ_n and γ_u represent the ratio of second derivative peaks (a/b; a denotes the arithmetic sum of $d^2A/d\lambda^2$ at 284.5 and 289 nm, and b denotes the arithmetic sum of $d^2A/d\lambda^2$ at 292 and 296 nm; Figure 7A) in native and denatured (6 M guanidine-HCl-treated) states, respectively. The second derivative peak ratio, γ_a, of free Tyr and Trp residues, in the same molar ratio as in the BoNT, is calculated based on the following equation (*16*):

$$\gamma_a = (Ax + B)/(Cx + 1)$$

where, A, B, and C are constants, −0.18, 0.64, and −0.04, respectively (*16*). x represents the molar ratio of Tyr and Trp in the polypeptide chain of BoNT/A; it is calculated to be 4.933 on the basis of the published amino acid sequence of BoNT/A (*18, 19*).

Table 1: Zn^{2+} Content of Holo-, Apo-, and Zn^{2+}-Replenished Type A Botulinum Neurotoxin

neurotoxin	Zn^{2+}/neurotoxin
holo-	0.92 ± 0.11
apo-	−0.12 ± 0.24
Zn^{2+}-replenished	
1:1	0.58 ± 0.19
1:5	0.93 ± 0.20
1:10	1.61 ± 0.14

Protein Unfolding. Temperature-induced unfolding of BoNT/A polypeptide was followed by monitoring the change with temperature in the CD signal at 222 nm. Holo-, apo-, and Zn^{2+}-replenished BoNT/A samples each dissolved in HPLC-grade water were heated with ellipticity recorded at 222 nm at every 0.1 °C between 25 and 100 °C. The rate of heating was 2 °C/min, and the entire far-UV CD spectrum (260−170 nm) was also recorded at every 5−10 °C temperature interval. Thermodynamic parameters were estimated for unfolding based on signal changes at 222 and 208 nm.

RESULTS

Reversibility of Zn^{2+}-Binding with BoNT. To understand the basis of irreversible structural changes as well as function, we analyzed the reversibility of Zn^{2+}-binding to BoNT/A. Analysis of Zn^{2+} content of holo-, apo-, and Zn^{2+}-replenished BoNTs with atomic absorption spectrometry revealed that the holo-BoNT contains one Zn^{2+}/molecule, which is consistent with earlier literature reports (*10*). Treatment with EDTA completely removed the bound Zn^{2+} to yield apo-BoNT. Incubation of apo-BoNT with Zn^{2+} in a 1:1 ratio did not refurbish the apo-BoNT but at 1:5 molar excess of Zn^{2+}, the BoNT was able to restore its Zn^{2+} content (Table 1). At a 1:10 molar excess, apparently more than one Zn^{2+} was bound to over 60% of the molecules of BoNT/A.

Biological Activity of BoNT. Biological activity of BoNT/A was assayed by monitoring BoNT-induced inhibition of Ca^{2+}-activated [^{3}H]norepinephrine release from permeabilized PC12 cells. In the absence of any BoNT, norepinephrine release was 48 ± 5%. [^{3}H]NE release was progressively inhibited with increasing concentration of the holo-BoNT/A (Figure 1a). At a concentration of 300 nM, holo-BoNT/A reduced the norepinephrine release to 30 ± 3%, resulting in a 38% inhibition of the neurotransmitter release. In contrast, apo-BoNT/A at 300 nM concentration reduced the norepinephrine release from 48 ± 5% to 44 ± 2%, a mere 8% blockage (Figure 1a) which is within the experimental error. Replenishment of apo-BoNT/A with different molar excess concentrations of Zn^{2+} did not seem to restore the biological activity of apo-BoNT/A (Figure 1b). Incubation with even 1 mM Zn^{2+} (a 2700-fold molar excess to the apo-BoNT/A) did not restore the ability of apo-BoNT/A to block norepinephrine release from PC12 cells.

Secondary Structure. Secondary structures of BoNT/A, apo-BoNT/A, and Zn^{2+}-replenished BoNT/A were determined by FT-IR and CD spectroscopy. FT-IR spectra of BoNT/A samples are shown in Figure 2. While the amide I band did not indicate any significant differences between BoNT/A and apo-BoNT/A, amide III indicated considerable increase in strength of 1315 cm^{-1} for apo-BoNT/A (Figure

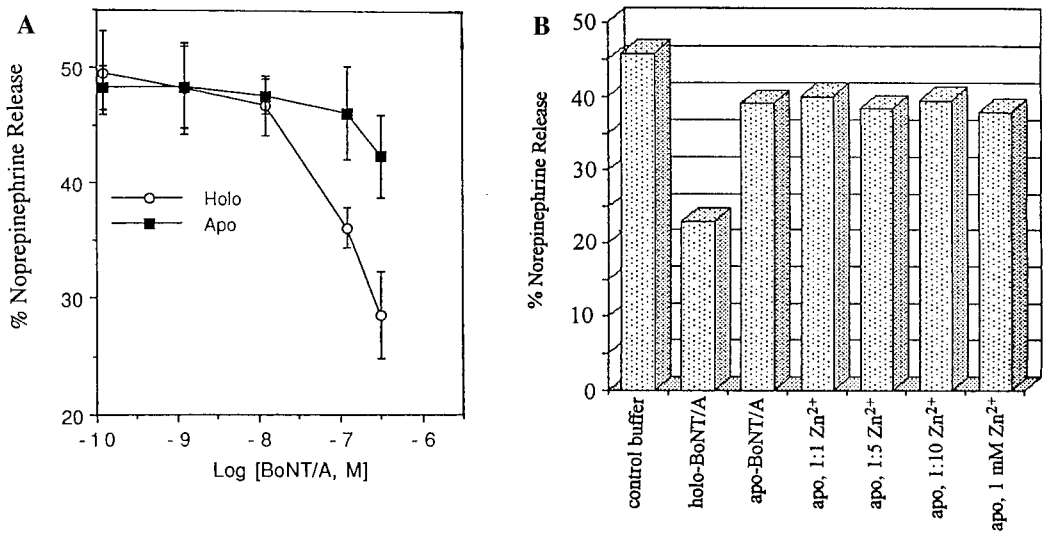

FIGURE 1: (A) Concentration-dependent inhibition of Ca^{2+}-activated [^{3}H]NE release from permeabilized PC12 by holo- and apo-BoNT/A. Permeabilized PC12 cells were incubated with 2 mM MgATP, rat brain cytosol, and BoNT/A (or control buffer) for 5 min at 30 °C. Ca^{2+} (1 μM) was added to triggered the exocytosis for 15 min at 30 °C. (B) Zn^{2+}-replenished BoNT/A. Apo-BoNT/A (3×10^{-7} M) was incubated with different molar excesses of Zn^{2+} for 33 min at 37 °C before loading into the permeabilized PC12 cells.

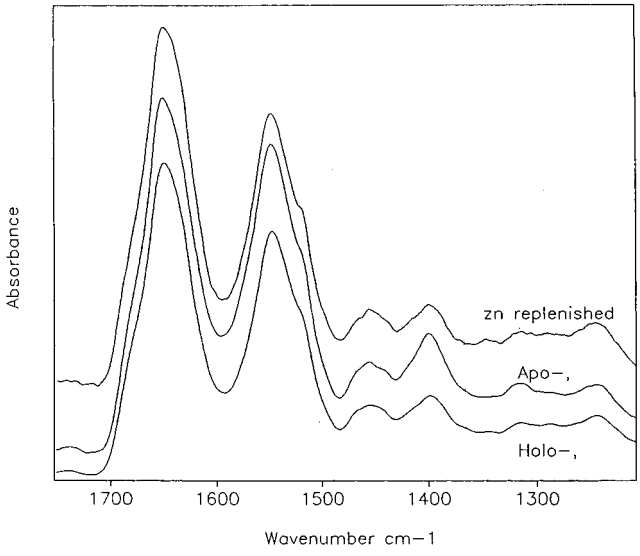

FIGURE 2: IR spectra of holo-, apo-, and Zn^{2+}-replenished (replenishment with 5-fold molar excesses Zn^{2+}) BoNT/A. Spectra were coadded using a 60° horizontal ZnSe ATR crystal with 1 mg/mL BoNT/A at room temperature (25 °C). Spectra are shown after subtraction of the buffer spectrum.

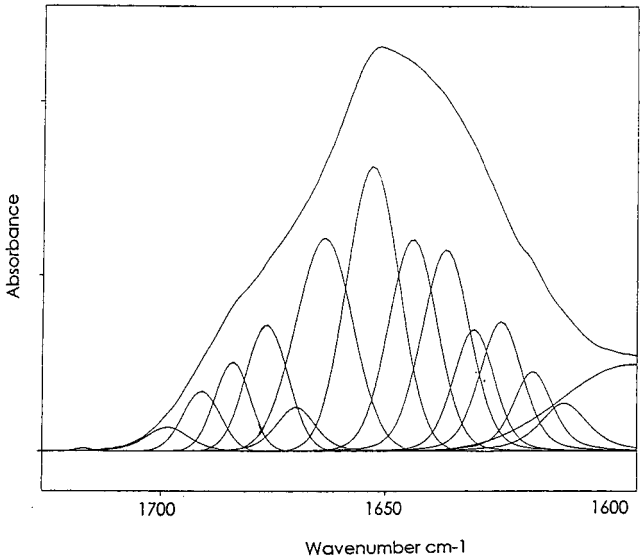

FIGURE 3: Curve-fitted IR spectrum of holo-BoNT/A in amide I spectral region. The curve-fitted spectrum was generated using a γ factor of 2.4 and filter factor of 0.36, as described in Materials and Methods.

2). Reincubation of the apo-BoNT/A with a 5-molar excess of Zn^{2+} resulted in an apparent reversal of the spectral features in the amide III region (Figure 2). A typical example of curve-fitting analysis of the amide I band (Figure 3) and subsequent assignment of resulting underlying bands to specific secondary structures (*14*) provided estimation of secondary structure contents (Table 2). Table 3 presents estimation of the average content of secondary structure from three separate analyses. Accurate resolution of amide I bands is difficult and subjective because of the generally featureless contour of the spectral band (*14*). The situation becomes more acute for proteins that have significant amounts of α-helix, β-sheets, β-turn, and random coil structures, as such conditions present more overlapping bands making assignments less reliable. Amide III band, on the other hand, contains more features even in its originally recorded spectrum (*14*, *21*). Amide I band analysis, therefore, is presented for comparative examination of changes in the resolved bands of BoNT/A after removal and replenishment of Zn^{2+}. Although removal of Zn^{2+} resulted in significant changes in the individual band strengths (Table 2), the overall estimation of secondary structure content did not seem to change (Table 3). The data in the curve-fitting analysis of amide III band (Table 4; Figure 4) also provided the estimated secondary structure content of holo-BoNT/A to be 29 ± 4% α-helix, 44 ± 3% β-sheets, and 27 ± 5% random coils and others (Table 3). Amide III band analysis of apo-BoNT/A revealed considerable change in the secondary structure content upon removal of Zn^{2+} (Table 3). For example, the α-helix content increased from 29% to 42%, and β-sheet content in apo-BoNT/A decreased from 44% to 36% (Table 3). Treatment of apo-BoNT/A with Zn^{2+} (1:1 molar ratio) did not seem to restore structural changes introduced by the removal of Zn^{2+} (Table 3). However,

Table 2: The Resolved Underlying Band Positions and Their Corresponding Secondary Structures of Representative BoNT/A IR Spectra in Amide I Region[a]

BoNT/A	band position	band percentage	assignment
holo-	1624	8.3	β-sheet
	1630	7.3	β-sheet
	1636	13.9	β-sheet
	1644	14.4	random coil
	1653	20.4	α-helix
	1664	16.7	turn
	1670	2.8	β-sheet/turn
	1677	7.2	β-sheet
	1684	4.3	turn
	1691	3.1	turn
	1698	1.6	turn
apo-	1622	2.6	β-sheet
	1629	21.6	β-sheet
	1639	11.9	random/β-sheet
	1644	5.8	random coil
	1651	19.6	random/α-helix
	1661	17.2	α-helix/turn
	1670	6.2	β-sheet/turn
	1676	4.8	β-sheet
	1682	4.3	turn
	1689	5.2	turn
	1698	0.6	turn
ReZn	1625	7.2	β-sheet
(1:5)	1631	9.1	β-sheet
	1638	15.5	β-sheet
	1646	15.4	random coil
	1654	15.1	α-helix/random
	1661	8.4	turn
	1669	13.2	turn/β-sheet
	1676	6.5	β-sheet
	1684	8.1	turn
	1693	1.6	turn

[a] Integrated band intensity was used for the calculation of the secondary structural content. The assignment of the resolved bands was based on Byler and Susi (*20*) and Fu et al. (*14*).

incubation of the apo-BoNT/A with a 5-fold molar excess of Zn^{2+} apparently restored the secondary structure of the BoNT/A (α-helix to 31%, β-sheets to 40%, β-turn/random coils to 29%; Table 3). Incubation with 1:10 molar excess of Zn^{2+} introduced structural changes that seemed to reflect an additional effect of Zn^{2+}-binding. For example, α-helix content remained 39%, whereas β-sheets content decreased from 36% to 32% (Table 3). The differential responses to incubation with 1:5 and 1:10 molar excesses of Zn^{2+} were unexpected.

Far-UV CD spectra of holo-BoNT/A, apo-BoNT/A, and Zn^{2+}-replenished BoNT/A are shown in Figure 5. The holo-BoNT/A CD spectrum showed a broad negative minimum at 208−222 nm and a positive CD maximum at 193 nm. No significant spectral changes were observed upon removal of Zn^{2+}, except for a noteworthy decrease at 193 nm (Figure 5). Replenishment of apo-BoNT/A with 1:5 molar excess Zn^{2+} did not result in any restoration of the spectral change observed above. Secondary structure estimation using the method of Sreerama and Woody (*15*) revealed 36 and 33% α-helix, 38 and 51% β-sheets, 8 and 4% β-turns, and 18 and 12% random coils, respectively, for holo-BoNT and apo-BoNT (Table 5).

Tertiary Structure. Comparative tertiary structural folding of holo-, apo-, and Zn^{2+}-replenished BoNT were analyzed in terms of topography of aromatic amino acid residues (near-UV CD and second derivative UV spectroscopy) and in terms of thermal unfolding.

Near-UV CD spectrum of holo-BoNT/A showed three major negative CD bands at 295, 288, and 270 nm and a shoulder at 280 nm (Figure 6). Removal of Zn^{2+} altered the spectral pattern substantially with decrease in the CD signal at 295 nm (14%) and increase in the CD signal at 270 (34%) and 280 nm (12%) (Figure 6). Incubation of apo-BoNT with 1:1 Zn^{2+} resulted in a general decrease of about 18% in the CD signal (Figure 6). Incubation of the apo-BoNT/A with 1:5 and 1:10 molar excesses of Zn^{2+} did not result in substantially different spectra from those obtained after incubation with 1:1 (molar) Zn^{2+}, except about an 11% decrease in the signal at 270 nm. In summary, the near-UV CD spectral analysis indicated that while CD signals of aromatic amino acid residues were considerably altered upon removal of Zn^{2+}, the spectral changes were not reversible upon replenishment of the Zn^{2+}.

The second derivative UV absorption spectrum of holo-BoNT/A is shown in Figure 7a. The spectrum exhibited the typical second derivative negative and positive peaks of proteins (*16*, *17*) at 284, 289, 293, and 296 nm. Second derivative spectra of apo-BoNT/A and Zn^{2+}-replenished BoNT/A with 1:1, 1:5, and 1:10 molar excesses Zn^{2+} did not reveal spectral features different from those of holo-BoNT/A (Figure 7b). Degree of Tyr exposure estimation after comparing the second derivative spectra of different native BoNT samples with those of their respective denatured samples revealed that about 90% of Tyr residues of BoNT/A are exposed to polar solvent environment (Table 6). Tyrosine exposure was not affected either by removal of Zn^{2+} or by replenishment of apo-BoNT/A with Zn^{2+}.

Polypeptide folding of the holo-, apo-, and Zn^{2+}-replenished BoNT/A was further analyzed by examining their folding and unfolding patterns as a function of temperature. Unfolding of the neurotoxin was followed by monitoring CD signal changes at 222 nm. The holo-BoNT/A showed a typical polypeptide unfolding curve (Figure 8). The protein unfolding started at 50 °C, and the neurotoxin was completely unfolded before the temperature reached 60 °C. The midpoint transition temperature for the holo-neurotoxin was estimated at 53 °C. Heating of apo- and Zn^{2+}-replenished BoNT/As did not show any significant change at 222 nm (Figure 8), suggesting a drastic difference in the polypeptide folding of the holo- and apo-BoNT/As, which was not reversed upon replenishing the apo-BoNT/A with Zn^{2+}. We further examined the far-UV CD spectra of holo-, apo-, and Zn^{2+}-replenished BoNT/As at different temperatures (Figure 9). It was observed that the holo-BoNT was denatured upon heating, whereas apo- and Zn^{2+}-replenished BoNTs retained their secondary structures (35% α-helix, 46% β-sheets, 7% β-turns, and 12% random coils) even after heating them to 100 °C. However, there were visible changes in the spectral recordings of both apo- and Zn^{2+}-replenished BoNT/A upon heating (Figure 9). We examined CD signal changes at 208 nm to monitor the progress of temperature-induced alteration in the structure of apo- and Zn^{2+}-replenished BoNT/A (Figure 10). For comparative purposes, we also monitored the CD signal change at 208 nm as a function of temperature for holo-BoNT/A also (Figure 10). Clearly, holo-BoNT/A showed a typical polypeptide unfolding curve where the unfolding seemed to have been completed by about 58 °C. However, unfolding patterns of apo-BoNT/A and Zn^{2+}-replenished BoNT/A indicated that the structural changes

Table 3: Secondary Structure Estimation of Type A Botulinum Neurotoxin at Various Zinc Binding States Based on the Curve-Fitting Results of the Amide I and Amide III IR Spectral Region

	amide I			amide III		
	α-helix/R.C.[a]	β-sheets	turns	α-helix	β-sheets	R. C./turns
holo-	38 ± 5	39 ± 4	23 ± 3	29 ± 4	44 ± 3	27 ± 5
apo-	42 ± 6	40 ± 4	20 ± 4	42 ± 3	36 ± 3	22 ± 5
Zn replenished[b]						
1:1	38 ± 5	42 ± 4	25 ± 4	39 ± 5	37 ± 4	25 ± 2
1:5	33 ± 7	40 ± 3	32 ± 1	31 ± 2	40 ± 2	29 ± 4
1:10	29 ± 3	49 ± 4	23 ± 1	39 ± 5	32 ± 1	28 ± 4

[a] R. C. represents random coils. [b] Indicates the molar ratio of botulinum neurotoxin to $ZnCl_2$ used for incubation.

Table 4: The Resolved Underlying Band Positions and Their Corresponding Secondary Structures of Representative BoNT/A IR Spectra in Amide III Region[a]

BoNT/A	band position	band percentage	assignment
holo-	1225	5.4	β-sheet
	1235	10.7	β-sheet
	1242	8.7	β-sheet
	1250	13.0	β-sheet
	1258	7.2	unordered
	1267	8.5	unordered
	1278	8.5	unordered
	1287	5.5	α-helix
	1296	8.4	α-helix
	1307	2.5	α-helix
	1317	22.1	α-helix
apo-	1236	2.0	β-sheet
	1243	15.2	β-sheet
	1252	9.2	β-sheet
	1259	7.2	β-sheet
	1268	6.0	unordered
	1281	10.9	unordered
	1290	9.2	unordered
	1303	7.9	α-helix
	1312	8.1	α-helix
	1319	24.8	α-helix
ReZn	1230	2.4	β-sheet
(1:5)	1237	12.7	β-sheet
	1245	9.1	β-sheet
	1251	8.3	β-sheet
	1257	11.3	β-sheet
	1264	3.1	unordered
	1272	8.5	unordered
	1280	1.9	unordered
	1287	11.0	unordered
	1296	5.0	α-helix
	1306	12.9	α-helix
	1316	9.1	α-helix
	1322	4.7	α-helix

[a] Integrated band intensity was used for the calculation of the secondary structural content. The assignment of the resolved bands was based on Fu et al., (1994).

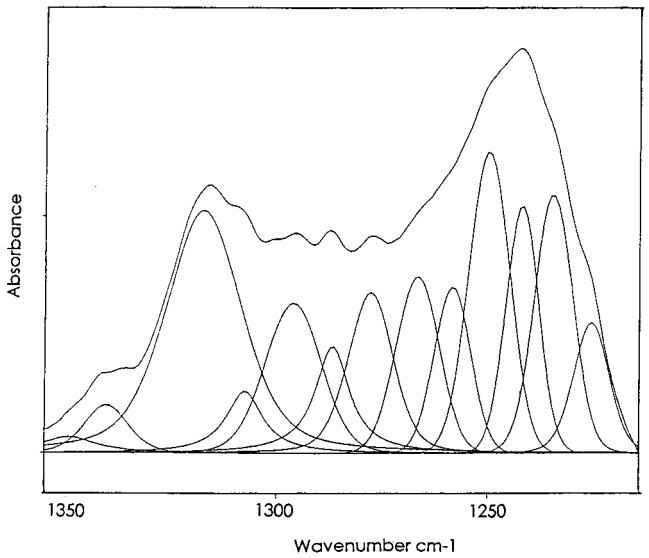

FIGURE 4: Curve-fitted IR spectrum of holo-BoNT/A in amide III region. The curve-fitted spectrum was generated using a γ factor of 2.5 and filter factor of 0.34, as described in Materials and Methods.

were maintained up to 100 °C. The signal change at 208 nm could not be used for thermodynamic analysis because the signal change did not reach a plateau to assume reaching complete structural change. It was still possible, however, to compare the unfolding pattern of apo-BoNT/A with Zn^{2+}-replenished BoNT/A by comparing the slopes of change at 208 nm CD signals between 60 and 100 °C, which were estimated to be identical (0.13 θ/°C).

DISCUSSION

The presence of bound Zn^{2+} in BoNTs has been shown to be critical for its biological activity of the blockage of neurotransmitter release in *Aplysia* neurons (*22*). However, we have demonstrated similar qualitative results of the blockage of norepinephrine release in PC12 cells for the first time. Norepinephrine release from PC12 cells has been effectively used in the past to assay the biological activity of several serotypes of BoNT (*13*, *23*). The 38% inhibition of norepinephrine release by 300 nM BoNT/A compares to about 30% inhibition observed by other researchers at a similar concentration of BoNT/A (*13*, *24*). Our results confirm that the bound Zn^{2+} is essential for the biological activity of BoNT/A in PC12 cells. Removal of Zn^{2+} from BoNT/A resulted in the loss of its activity which was not restored with re-incubation of the apo-BoNT/A with excess Zn^{2+} (Figure 1). Because the Zn^{2+}-binding to BoNT/A itself is reversible (Table 1), it seems that removal of Zn^{2+} perhaps results in conformational changes which are not completely reversible under our experimental conditions. This contrasts with some earlier work. Irreversibility of Zn^{2+} removal of a BoNT/A L chain was observed by Schiavo et al. (*10*). Zn^{2+} removal experiments with BoNT/B have shown reversible enzymatic activity for its known proteolytic activity against synthetic polypeptides corresponding to synaptobrevin (a substrate for BoNT/B) (*25*). One explanation for our observation of irreversible loss of biological activity could be that different serotypes of BoNT have differential structural susceptibility to the loss of Zn^{2+}. In another set of experiments with BoNT/E, we observed the loss of activity upon removal of Zn^{2+} which could be partially restored (about 25%) upon replenishment with Zn^{2+} (unpublished

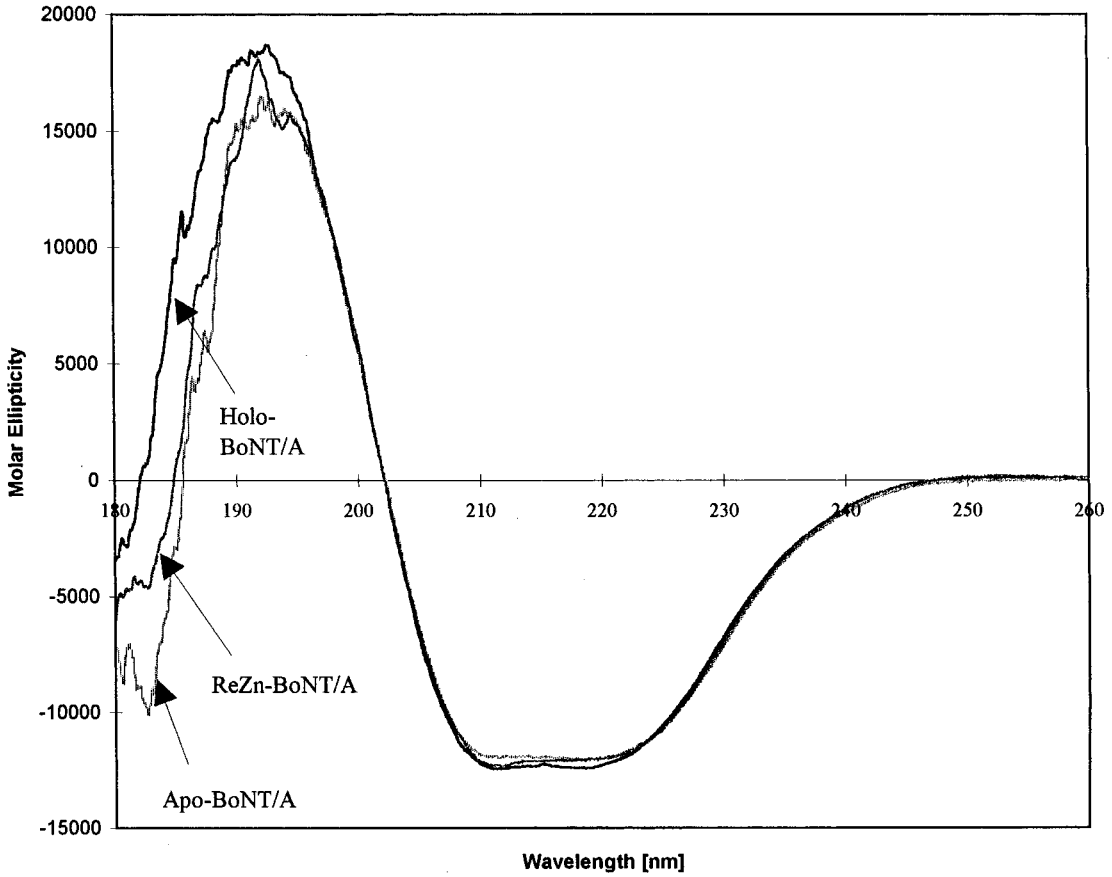

FIGURE 5: Far-UV CD spectra of holo-, apo-, and Zn^{2+}-replenished (with 5-fold molar excess) BoNT/A dissolved in water. All spectra were recorded at room temperature (25 °C) using a 1 mm path-length quartz cell with BoNT/A concentrations in the range of 0.1−0.2 mg/mL. Spectral recordings were carried out at a scan rate of 20 nm/min with 8 s response time. Spectra were adjusted for baseline.

Table 5: Secondary Structure Estimation of Type A Botulinum Neurotoxin in Its Holo-, Apo-, and Zn^{2+}-Replenished States

neurotoxin	α-helix	β-sheets	β-turns	others
holo-	36 (36)[a]	38 (38)	8 (9)	18 (18)
apo-	33 (35)	51 (49)	4 (2)	12 (14)
Zn^{2+}-replenished				
1:5	27 (30)	46 (44)	9 (12)	19 (15)

[a] The numbers in parentheses reflect the results of repeat sets of experiments.

data). The target protein for BoNT/A and BoNT/E is the same synaptic membrane protein (SNAP-25) which makes such a comparison appropriate. Two other clostridial neurotoxins, BoNT/B and tetanus neurotoxin (TeNT), which share an identical synaptic target protein and cleavage site differ in their sensitivity to temperature, pH, dithiothreitol, and Zn^{2+} concentration (*25*).

The loss of biological activity with the removal of Zn^{2+} was accompanied by significant structural changes at the secondary structure level as revealed by FT-IR spectroscopy but not by far-UV CD (Tables 2−4). The overall estimation of secondary structural features based on the amide I band analysis of IR spectra or far-UV CD spectral analysis did not reveal substantial structural changes, and the general pattern of the structural features derived from the two techniques were similar (Tables 3 and 5). However, both amide I IR and far-UV CD spectral analysis have inherent deficiencies in resolving localized structural changes. For the amide I band, the recorded spectra are generally featureless, and distinction of predominant secondary structural features is difficult unless the protein is all a or all b (*14*). While the overall estimation of secondary structural features from amide I spectrum remained largely unchanged upon removal of Zn^{2+}, resolved spectral band assignments (Figure 3 and Tables 2 and 3) indicate substantial changes in individual band strengths (for example, compare the band strengths at 1644 and 1629/1630 cm^{-1} bands of holo- and apo-BoNT/A; Table 2). In case of far-UV CD, the spectral features associated with secondary structural components are not as spatially resolved as the IR bands because of the overlapping nature of $n-\pi$ and $\pi-\pi$ transitions of amide carbonyl group and because of an intrinsic insensitivity of electronic spectra, compared to vibrational spectra, to minute variations in the vicinity of participating chromophores in the secondary structure folding of proteins.

Amide III spectral features clearly indicated structural changes in BoNT/A upon Zn^{2+} removal (Figure 2 and Tables 3 and 4), most prominently in the α-helical structures. The amide III spectral region has been demonstrated to be more sensitive to the secondary structures of proteins than the amide I region (*14*). Attempts to regenerate the holo-BoNT/A secondary structure by incubating it with different molar excesses of Zn^{2+} seemed to succeed only at 1:5 (BoNT/A: Zn^{2+}, mol/mol) ratio (Table 3). Incubation of apo-BoNT/A with Zn^{2+} at higher molar ratio (1:10) resulted in additional structural changes (Table 3). Under all three experimental conditions (incubation of apo-BoNT/A with excess Zn^{2+} at 1:1 or 1:10 BoNT/A: Zn^{2+} molar ratio), biological activity of Zn^{2+}-treated apo-BoNT/A was not

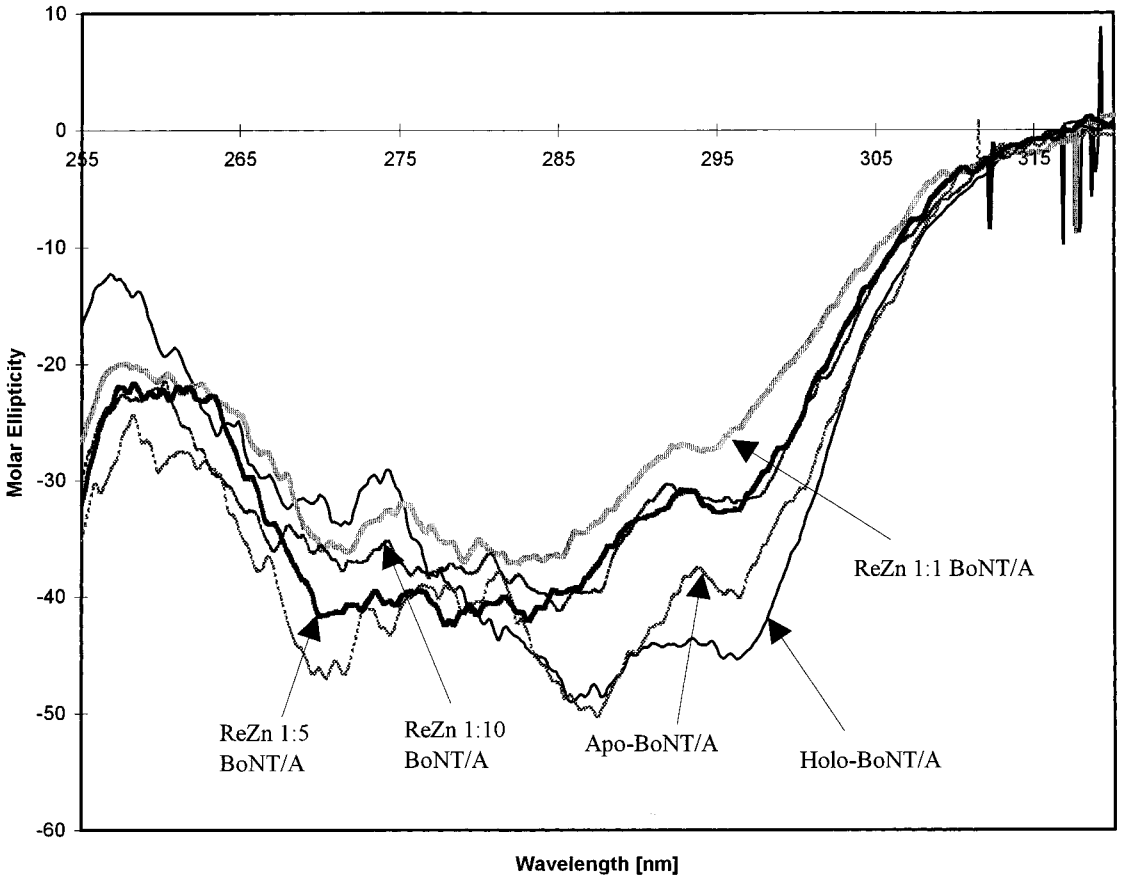

FIGURE 6: Near-ultraviolet CD spectra of holo-, apo-, and Zn^{2+}-replenished (ReZn) BoNT/A dissolved in water. Zn^{2+}-replenished BoNT/A was prepared by incubating apo-BoNT/A with 1:1, 1:5, and 1:10 molar excess of $ZnCl_2$. All spectra were recorded at room temperature (25 °C). Spectral recordings were carried out at a scan speed of 20 nm/min and a response time of 8 s. Each spectrum was obtained after subtracting the buffer spectrum.

restored. This was true irrespective of whether the secondary structure of the Zn^{2+}-treated apo-BoNT/A was similar to holo-BoNT/A secondary structure.

Our analysis of Zn^{2+} uptake during our regeneration attempts suggested that incubation of apo-BoNT/A with Zn^{2+} in a 1:1 molar ratio allowed on average uptake of Zn^{2+} by about 60% BoNT molecules (Table 1). However, a 1:5 and 1:10 molar excess of Zn^{2+} resulted in the uptake of about one Zn^{2+} and over 1.5 Zn^{2+}, respectively, per BoNT/A molecule. Therefore, biological activity of apo-BoNT/A was not restored with Zn^{2+} incubation despite the binding of Zn^{2+}. At 1:10 molar excess, more than one Zn^{2+} seemed to bind to BoNT/A molecules. The binding at an additional site might induce structural changes observed at the secondary structural level (Table 3). While we have not determined the binding site of Zn^{2+} to apo-BoNT/A in our experiments, it seems logical to assume that the initial binding occurs at the high-affinity zinc binding motif present in BoNT/A and other serotypes of BoNT, and the additional Zn^{2+}-binding might occur at an as yet unidentified weak binding site (*10*). For a catalytic role of Zn^{2+} in the BoNT/A endoprotease activity (*9*−*11*), Zn^{2+}-binding to the high-affinity binding site should be sufficient. Nonrestoration of biological activity despite Zn^{2+}-binding and apparent restoration of secondary structure (at 1:5 molar ratio) could indicate that the BoNT tertiary structure may have irreversibly changed upon the removal of Zn^{2+}.

Tertiary structural changes were estimated by monitoring topography of aromatic amino acid residues and thermal unfolding of BoNT. The degree of Tyr exposure estimated by second derivative UV absorption spectroscopy revealed virtually no change in the surface topography of Tyr upon removal of Zn^{2+} (Table 6). The degree of Tyr exposure of BoNT/A estimated in this study was very similar to the one obtained previously (84%; *26*). While it seems that most Tyr residues are exposed to aqueous solvent at the protein surface (*16*, *26*), it is possible that some of these residues are exposed to either patches of aqueous solvent or to other charged residues within the protein matrix. In any case, no net alteration in the topography of Tyr residues was observed in BoNT/A upon the removal of Zn^{2+}. Therefore, we employed a different technique, near-UV CD spectroscopy, to examine changes in the Tyr and other aromatic amino acid residues.

Near-UV CD signals of aromatic amino acid residues are sensitive to topographical and environmental changes in their vicinity (*17*, *27*−*29*). The band at 270 nm, which showed the strongest change upon removal of Zn^{2+} (Figure 6), can be assigned to Phe residues, whereas the band observed at 280 nm can be assigned to the ^1L_b band of Tyr residues (*17*). While the band at 288 nm could also arise from Tyr residues, we believe it arises due to the ^1L_a band of Trp residues based on our previous analysis (*17*). The 295 nm band clearly originates from ^1L_b transitions. Substantial spectral changes corresponding to all three aromatic amino acid residues certainly indicate significant changes in the polypeptide folding of BoNT/A upon the removal of Zn^{2+}. However, the most prominent change at 270 nm suggests a strong

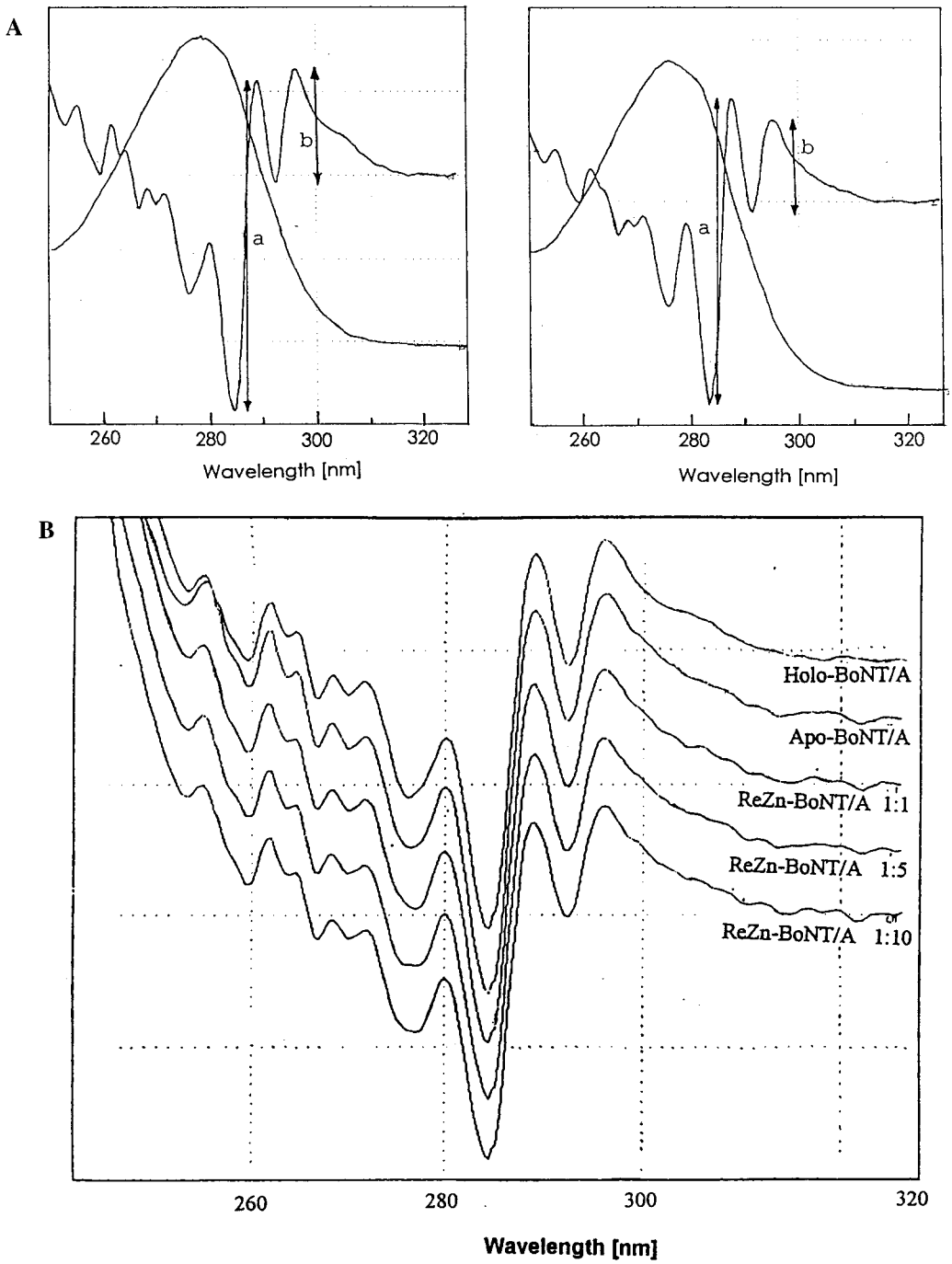

FIGURE 7: (A) Absorption and second derivative spectra of holo-BoNT/A dissolved in 150 mM Tris-HCl buffer, pH 7.4 (left panel) and in 6 M guanidine-HCl (right panel). *a* denotes the arithmetic sum of $d^2A/d\lambda^2$ at 284.5 and 289 nm. *b* denotes the sum of $d^2A/d\lambda^2$ at 292 and 296 nm. (B) Second derivative absorption spectra of holo-, apo-, and Zn^{2+}-replenished (with different molar excesses of Zn^{2+}) BoNT/A. Five independent absorption spectra were scanned at 50 nm/min rate with a spectral bandwidth of 0.3 nm for each sample. An average spectrum was then obtained before obtaining derivative spectra.

alteration in the polypeptide folding near Phe residues. There are 52 Phe residues in BoNT/A, 27 of which are located in the light chain (*18*, *19*). Five L chain Phe residues (Phe-188, Phe-192, Phe-194, Phe-196, and Phe-213) are located in the vicinity of the zinc binding motif 223-HEXXH, which could be contributing to the near-UV CD signal. Because our second derivative UV absorption spectral analysis did not reveal any overall change in the surface topography of Tyr residues (vide supra), we believe the changes in the Tyr residues revealed by near-UV CD spectroscopy suggest changes in the vicinity of those Tyr residues that are embedded in the protein matrix. It is notable that strong CD signals are maintained despite the removal of Zn^{2+}. Attempted regeneration of holo-BoNT/A by incubation with excess Zn^{2+} seemed to restore the spectral changes, but it was not able to regenerate the original holo-BoNT/A CD spectrum. Taken together, these observations suggested that the biological activity irreversibly lost due to the removal of Zn^{2+} was very sensitive to the structural changes in BoNT/A. Conversely, bound Zn^{2+} may play a considerable role in the maintenance of the biologically active structure of BoNT/A.

Thermal unfolding characterizitics of BoNT/A in the presence and absence of bound Zn^{2+} provided perhaps the

Table 6: Degree of Tyr Exposure in Holo-, Apo-, and Zn^{2+}-Replenished BoNT/A by Second Derivative UV Absorbance Spectroscopy

neurotoxin	γ_n[a]	degree of Tyr exposure[b]
holo-	3.13 ± 0.02	90.3 ± 3.5%
apo-	3.14 ± 0.07	90.5 ± 2.4%
Zn^{2+}-replenished		
1:1	3.00 ± 0.06	86.9 ± 3.8%
1:5	3.15 ± 0.04	90.8 ± 2.4%
1:10	3.09 ± 0.05	89.2 ± 5.1%

[a] Values represent an average of 5 different sets of experiments, each with five spectral recordings. Standard deviations are for a given set of spectral recordings. [b] γ_u used was 3.50 ± 0.09 (n = 9). Standard deviations are calculated for the degree of Tyr exposure for the five different sets of determinations.

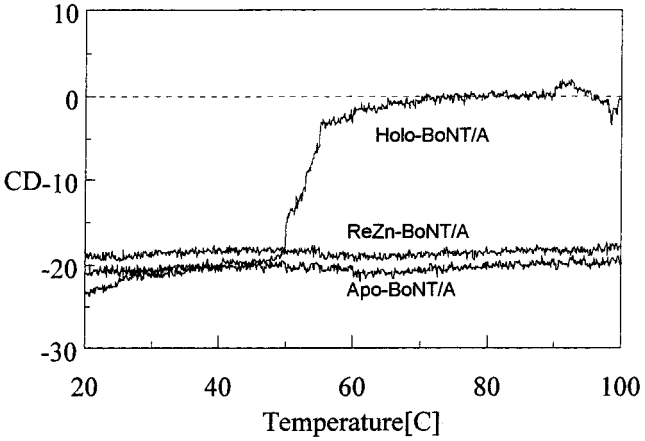

FIGURE 8: Thermal unfolding of holo-, apo-, and Zn^{2+}-replenished BoNT/A (with 5-fold molar excess of Zn^{2+}). Samples were heated from 25 to 100 °C at a heating rate of 2 °C/min. The unfolding was monitored by recording CD signal at 222 nm with 0.1 °C resolution.

most dramatic evidence of a polypeptide folding change induced by Zn^{2+} removal. The inverse Z-shaped unfolding curve largely indicated a two-state unfolding of holo-BoNT/A. However, the protein was precipitated after the heating cycle, suggesting irreversibility of the unfolding. Such a behavior was not unexpected of a protein with 150 kDa and known functional domains. The unfolding curve also showed an indication of more than single cooperative unfolding. Reversible polypeptide unfolding is generally observed only with relatively small proteins (*30*, *31*). To estimate thermodynamic parameters of protein unfolding, it is assumed that the process occurs as a single cooperative phenomenon. Therefore, it was not appropriate to calculate true thermodynamic parameters (ΔG, ΔH, and ΔS). Calculation of pseudo thermodynamic parameters using a method described in the literature (*32*) revealed values of 223 kcal/mol, 685 cal mol^{-1} K^{-1}, and 19 kcal/mol for ΔH, ΔS, and ΔG, respectively, which are similar to those of other known proteins analyzed for similar parameters (*32*).

The absence of clear denaturation transition either in apo-BoNT/A or in Zn^{2+}-replenished BoNT/A could be explained by assuming a molten globule-type structure for these proteins. In molten globule structures, secondary structures are generally preserved and tertiary structures are also flexible (*33*). While the estimated secondary structure did not seem to change significantly, the spectral shapes of both apo- and Zn^{2+}-replenished BoNT/A were considerably changed at 100

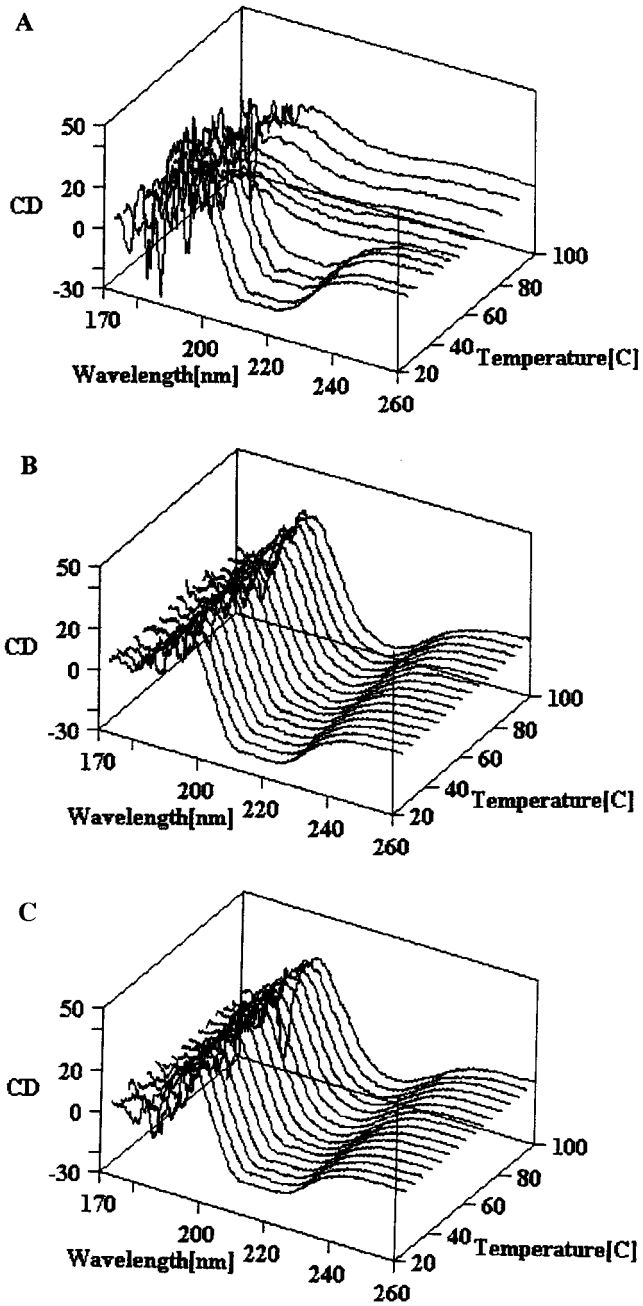

FIGURE 9: Far-UV CD spectra of (A) holo-BoNT/A, at different temperatures. The spectra were recorded along with the thermal unfolding process described at Figure 8. The spectral scan rate was set at 20 nm/min with response time at 8 s. The spectral scanning was carried every 5 °C from 25 °C to 100 °C. (B) Far-UV CD spectra of apo-BoNT/A, at different temperatures. Conditions were the same as described in (A). (C) Far-UV CD spectra of Zn^{2+}-replenished (with 5-fold molar excess of Zn^{2+}) BoNT/A at different temperatures.

°C, compared to lower temperatures as shown by a single extremum at 215 nm rather than double minima at 221 and 210 nm (Figure 9). These observations suggest that (*1*) Zn^{2+} must be playing a critical role in the maintenance of BoNT/A structure, in addition to its catalytic role, and (*2*) removal of Zn^{2+} irreversibly denatures BoNT/A.

The structural role of Zn^{2+} was recently examined in TeNT L chain (*34*). That study suggested little structural role of Zn^{2+} in the TeNT L chain based on far-UV CD, intrinsic fluorescence, and second derivative spectroscopy. In our

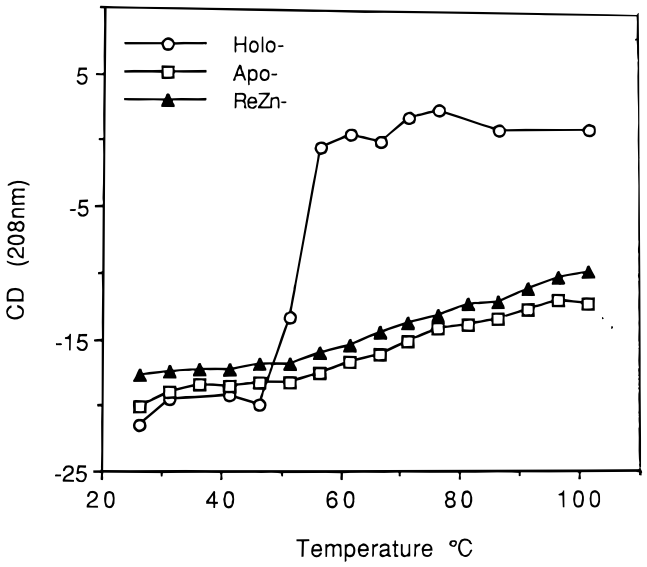

FIGURE 10: Thermal unfolding of holo-, apo-, and Zn^{2+}-replenished BoNT/A (with 5-fold molar excess of Zn^{2+}) monitored at 208 nm. The curves were constructed using CD signal obtained from Figure 9 at 208 nm.

study with BoNT/A, however, we have observed a mixed set of results. Far-UV CD and second derivative spectroscopic analysis did not reveal substantial structural changes. In addition, intrinsic fluorescence spectra of holo- and apo-BoNT/A were identical (F.-N. Fu and B. R. Singh, unpublished results). But FT-IR analysis and tertiary structure folding parameters (near-UV CD and thermal denaturation) indicated dramatic changes in structure of BoNT/A upon removal of Zn^{2+}. It is possible that BoNT/A and TeNT differ in their response to Zn^{2+} removal. Furthermore, the TeNT study was carried out with isolated L chain that was not amenable to Zn^{2+} re-uptake (*34*) in contrast to 150 kDa TeNT or BoNT/A, suggesting that the isolated TeNT L chain could behave structurally differently compared to the L chain attached to the H chain of the neurotoxin. Previous studies have suggested significant changes in the polypeptide folding of L and H chains of BoNT/A upon their separation (*17*, *26*).

Several studies have indicated that removal of Zn^{2+} with the use of chelators resulted in the loss of biological activities of BoNT/A, BoNT/B, and TeNT (*9*, *22*, *25*, *35*−*37*). Studies with EDTA treatment of BoNT and TeNT have elicited mixed results. For example, EDTA treatment effectively decreased BoNT/B and TeNT biological activities, but it was not effective in inhibiting proteolytic activity of BoNT/A against SNAP-25, the identified cellular target of BoNT/A (*22*). Our results thus demonstrated, for the first time, that BoNT/A biological activity could be reduced by treatment with EDTA (Figure 1). EDTA had been demonstrated to remove Zn^{2+} from BoNT/A in a reversible manner (*10*), a finding that is consistent with our results (Table 1). In an indirect study, chelators including EDTA did not have any adverse effect on BoNTs (including BoNT/A) when their activity was tested on neuromuscular junction tissue preparations (*38*). However, treatment of tissues with chelators did antagonize the neuromuscular blocking properties of BoNTs. The first set of results was explained in terms of re-uptake of Zn^{2+} present in tissues to reactivate BoNTs treated by chelators (*38*). Such an explanation could suggest that the biological activity of BoNTs can be restored by Zn^{2+}-binding, a finding that was not observed in our experimental conditions.

There has been no previous study of comparative testing of BoNT/A and apo-BoNT/A activity in PC12 cells. Our results with PC12 cells demonstrate that Zn^{2+} removal by EDTA resulted in the loss of inhibitory activity of BoNT/A in blocking the neurotransmitter release, and the inhibitory activity of BoNT/A could not be regenerated by incubation with excess Zn^{2+} even though such a treatment reestablished binding of Zn^{2+} to BoNT/A. Interestingly, the irreversible loss of biological activity of BoNT/A with Zn^{2+} removal was accompanied not only by structural changes but also with the irreversibility of structural changes to a large extent. Therefore, the structural changes observed are likely to be associated with the functional activity of the neurotoxin.

In previous reports, Zn^{2+} has been proposed to play a catalytic role, rather than a structural role, in clostridial neurotoxins (*5*, *11*, *34*). There is a zinc-binding motif (HExxH) present in all the serotypes of BoNT and in TeNT, and the two histidine residues are known to bind to Zn^{2+} (*10*). Two other residues involved in binding with Zn^{2+} are predicted to be located in the C-terminal segment of the L chain (*39*, *40*). It is, therefore, possible that Zn^{2+}-binding could induce conformational changes to accommodate binding of distal residues with Zn^{2+}. We do not know at this point the proper conditions involved in the proper incorporation of Zn^{2+} into BoNT/A, in vitro or in vivo, which will allow appropriate polypeptide folding for biological activity. It is possible that other proteins may be involved in vivo for correct folding of BoNT/A upon binding with Zn^{2+}. Further experiments with L chain and intact BoNT/A to understand the molecular basis of the structural and functional roles of Zn^{2+} are likely to provide critical information on the mechanism of clostridial endoprotease activity, which seems to represent a unique class of metalloproteases (*11*). There is no other known example of thermolysin-like Zn^{2+} protease such as BoNT where the metal plays both catalytic and structural roles (*41*). However, BoNTs are also the only group of Zn^{2+}-proteases with such a exclusive specificity for their respective substrates and their cleavage sites. Thus their unique characteristics vis-à-vis zinc's role is consistent with their unique substrate specificity.

In summary, our experimental data suggest that removal of Zn^{2+} from BoNT/A results in (i) irreversible loss of biological activity as assayed by neurotransmitter release in PC12 cells, and (ii) irreversible alteration in secondary and tertiary structures. The removal of Zn^{2+} itself is reversible, suggesting Zn^{2+} plays a structural role in addition to its catalytic role in BoNT/A.

REFERENCES

1. Simpson, L. L. (1981) *Pharmacol. Rev. 33*, 155−188.
2. Scott, A. (1989) in *Botulinum neurotoxin and tetanus toxin* (Simpson, L. L., Ed.) pp 399−412, Academic Press, San Diego, CA.
3. Bajjalieh, S. M., and Scheller, R. H. (1995) *J. Biol. Chem. 270*, 1971−1974.
4. Singh, B. R. (1996) Critical aspects of bacterial protein toxins, *Adv. Exp. Med. Biol. 391*, 63−68.
5. Montecucco, C., and Schiavo, G. (1994) *Mol. Microbiol. 13*, 1−8.

6. Simpson, L. L. (1993) in *Botulinum and tetanus neurotoxins* (DasGupta, B. R., Ed.) pp 5−16, Plenum Press, New York.
7. Hooper, N. H. (1994) *FEBS Lett. 354*, 1−6.
8. Vallee, B. L., and Auld, D. S. (1990) *Biochemistry 29*, 5647−5659.
9. Schiavo, G., Poulain, B., Rosetto, O., Benfenati, F., Tauc, L., and Montecucco, C. (1992) *EMBO J. 11*, 3577−3583.
10. Schiavo, G., Rosetto, O., Santucci, A., DasGupta, B. R., and Montecucco, C. (1992) *J. Biol. Chem. 267*, 23479−23483.
11. Montecucco, C., and Schiavo, G. (1993) *Trends Biochem. Sci. 18*, 324−327.
12. Fu, F.-N., Sharma, S. K., and Singh, B. R. (1998) *J. Protein Chem. 17*, 53−60.
13. Lomneth, R., Martin, T. F. J., and DasGupta, B. R. (1991) *J. Neurochem. 57*, 1413−1421.
14. Fu, F.-N., DeOliveira, D. B., Trumble, W. R., Sarkar, H. K., and Singh, B. R. (1994) *Appl. Spectrosc. 48*, 1432−1441.
15. Sreerama, N., and Woody, R. W. (1993) *Anal. Biochem. 209*, 32−44.
16. Ragone, R., Colonna, G., Balestrieri, C., Servillo, L., and Irace, G. (1984) *Biochemistry 23*, 1871−1875.
17. Singh, B. R., and DasGupta, B. R. (1990) *Biophys. Chem. 34*, 259−267.
18. Binz, T., Kurazono, H., Popoff, M. W., Frevert, J., Wernars, K., and Niemann, H. (1990) *J. Biol. Chem. 265*, 9153−9158.
19. Thompson, D. E., Brehm, J. K., Oultram, J. D., Swingfielk, T. J., Shone, C. C., Atkinson, T., Melling, J., and Minton, N. P. (1990) *Eur. J. Biochem. 189*, 73−81.
20. Byler, D. M., and Susi, H. (1986) *Biopolymers 25*, 469−487.
21. Singh, B. R., Fu, F.-N., and Ledoux, D. N. (1994) *Nat. Struct. Biol. 1*, 358−360.
22. Blasi, J, Chapman, E. R., Link, E., Binz, T., Yamasaki, S., DeCamilli, P., Sudhof, T., Niemann, H., and Jahn, R. (1993) *Nature 365*, 160−163.
23. Banerjee, A., Kowalchyk, J. A., DasGupta, B. R., and Martin, T. F. J. (1996) *J. Biol. Chem. 271*, 20227−20230.
24. Banerjee, A., Martin, T. F. J., and DasGupta, B. R. (1993) *Neurosci. Lett. 164*, 93−96.
25. Foran, P., Shone, C. C., and Dolly, J. O. (1994) *Biochemistry 33*, 15365−15374.
26. Singh, B. R., and DasGupta, B. R. (1989) *Mol. Cell. Biochem. 86*, 87−95.
27. Batenjany, M. M., Mizukami, H., and Salhany, J. M. (1993) *Biochemistry 32*, 663−668.
28. Strickland, E. H. (1974) *Crit. Rev. Biochem. 3*, 113−175.
29. Woody, R. W., and Dunker, A. K. (1996) in *Circular Dichroism and Conformational Analysis of Biomolecules* (Fasman, G. D., Ed.) pp 109−157, Plenum Press, New York.
30. Murphy, K. P., and Freire, E. (1992) *Adv. Protein Chem. 43*, 313−361.
31. Ganesh, C., Shah, A. N., Swaminathan, C. P., Surolia, A., and Vardarajan, R. (1997) *Biochemistry 36*, 5020−5028.
32. Kono, M., Sen, A. C., and Chakravarti, B. (1990) *Biochemistry 29*, 464−470.
33. Peng, Z., and Kim, P. S. (1992) *Biochemistry 33*, 2136−2141.
34. de Fillippis, V., Vangelista, L., Schiavo, G., Tonello, F., and Montecucco, C. (1995) *Eur. J. Biochem. 229*, 61−69.
35. Deshpande, S. S., Sheridan, R. E., and Adler, M. (1995) *Toxicon 33*, 551−557.
36. Sheridan, R. E., and Despande, S. S. (1995) *Toxicon 33*, 539−549.
37. Shone, C. C., Quinn, C. P., Wait, R., Hallis, B., Fooks, S. G., and Hambleton, P. (1993) *Eur. J. Biochem. 217*, 965−971.
38. Simpson, L. L., Coffield, J. A., and Bakry, N. (1993) *J. Pharmacol. Exp. Ther. 267*, 720−727.
39. Schiavo, G., Rossetto, O., Benfenati, F., Poulain, B., and Montecucco, C. (1994) *Ann. N.Y. Acad. Sci. 710*, 65−75.
40. Schiavo, G., Rosetto, O., and Montecucco, C. (1994) *Semin. Cell Biol. 5*, 221−229.
41. Lipscomb, W. N., and Sträter, N. (1996) *Chem. Rev. 96*, 2375−2433.

BI9723966